Influence of tectonic fractures zones on gravitational rock slope failures: New insights from 2-D physical modeling

T. Bois, S. Bouissou

JOURNAL OF GEOPHYSICAL RESEARCH, VOL. 115, F03009, doi:10.1029/2009JF001403, 2010

Influence of tectonic fractures zones on gravitational rock slope failures: New insights from 2-D physical modeling

T. Bois[1] and S. Bouissou[1]

Received 26 June 2009; revised 2 February 2010; accepted 22 February 2010; published 24 July 2010.

[1] Inherited structural discontinuities are known to play a dominant role in rock slope stability. The influence of their density and persistence on failure kinematics, resulting mobilized volume and slope morphology remains poorly constrained. The influence of these parameters is addressed using a 2-D physical modeling technique. Rather than undertaking a parametric analysis, we examine geologically stable model configuration based upon the well-documented landslide at Randa, Switzerland. The models consisted of a homogeneous material in which several fracture zones were introduced in order to study simplified but realistic configurations of discontinuities. Results showed that the type of gravitational failure (deep-seated landslide or sequential failure) and resulting slope morphology are very sensitive to the number and geometry of preexisting fracture zones. First, an increase in the density of fractures led to formation of the gravitational failure and increased the final mobilized volume. Second, fracture persistence exerted a strong control upon the kinematics of slope movements but had little influence on the final volume of the mobilized mass.

Citation: Bois, T., and S. Bouissou (2010), Influence of tectonic fractures zones on gravitational rock slope failures: New insights from 2-D physical modeling, *J. Geophys. Res.*, *115*, F03009, doi:10.1029/2009JF001403.

1. Introduction

[2] Rock slope stability is highly controlled by discontinuities such as bedding planes, foliation, faults or joints [*Terzaghi*, 1962; *Kato and Hada*, 1980; *Chigira*, 1985; *Agliardi et al.*, 2001]. Among these, faults and/or joints may develop and propagate under gravitational loading and lead the slope to a failure threshold [*Kaneko et al.*, 1997; *Sartori et al.*, 2003]. Rock slope stability is thus highly dependent on the large-scale mechanical behavior and strength of the rock mass, in which the number and persistence of preexisting fracture zones plays a significant role. In order to study such complex phenomena, numerical modeling has attempted to account for the influence of strength degradation on rock slope failure, primarily focusing upon simulation of brittle failure initiation [*Stead and Eberhardt*, 1997; *Eberhardt et al.*, 2004; *Stead et al.*, 2006]. Furthermore, the importance of fracture geometry, persistence and clustering has been demonstrated using probabilistic models [*Einstein et al.*, 1983], or with the displacement discontinuity boundary element method [*Scavia*, 1995]. Those modeling approaches however do not test the sensitivity of their results to the preexisting fracture zones' characteristics, in particular fracture density and persistence. We propose to address this question using a recently developed physical modeling technique [*Chemenda et al.*, 2005]; a method that is well suited to analyzing brittle failure [*Bachmann et al.*, 2006; *Bois et al.*, 2008; *Bachmann et al.*, 2009] and is here applied to study both failure initiation and propagation mechanisms. We demonstrate that the approach is capable of taking into account a large number of preexisting fractures zones into a single model. Our aim is therefore to study the influence of fracture density and persistence on the dynamics and evolution of gravitational rock mass failure. To do this, we start with a simplified but realistic (e.g., natural) configuration, rather than a parametric study, which allows direct comparison with observations made in the field. We performed 2-D scaled models based upon the 1991 Randa rockslide in Switzerland. The main assumptions made in our approach are as follows: (1) the rock mass is assumed to be homogeneous at the massive scale, (2) the large numbers of fractures observed in nature can be represented in a simplified model by a smaller number of "fracture zones," (3) the problem can be addressed in two dimensions. Even if physical models are inherently 3-D, we choose to neglect the complexity of the third dimension in the present study in order to compare our results directly with existing numerical models at this site [*Eberhardt et al.*, 2004; *Stead et al.*, 2006].

2. Geological Setting

[3] The 1991 Randa rockslides sequence was composed of two large volumes of rock (about 30 million m^3), falling between 18 April and 9 May. These rockslides have volumes characteristic of deep seated landslides, but the kinematics were observed to be quite different. Notably, deep seated failures are generally assumed to be slow with velocities of <1 Myr^{-1}, with effectively continuous sliding movement

[1]Géosciences Azur, UMR 6526, Université de Nice Sophia-Antipolis, Valbonne, France.

0148-0227/10/2009JF001403

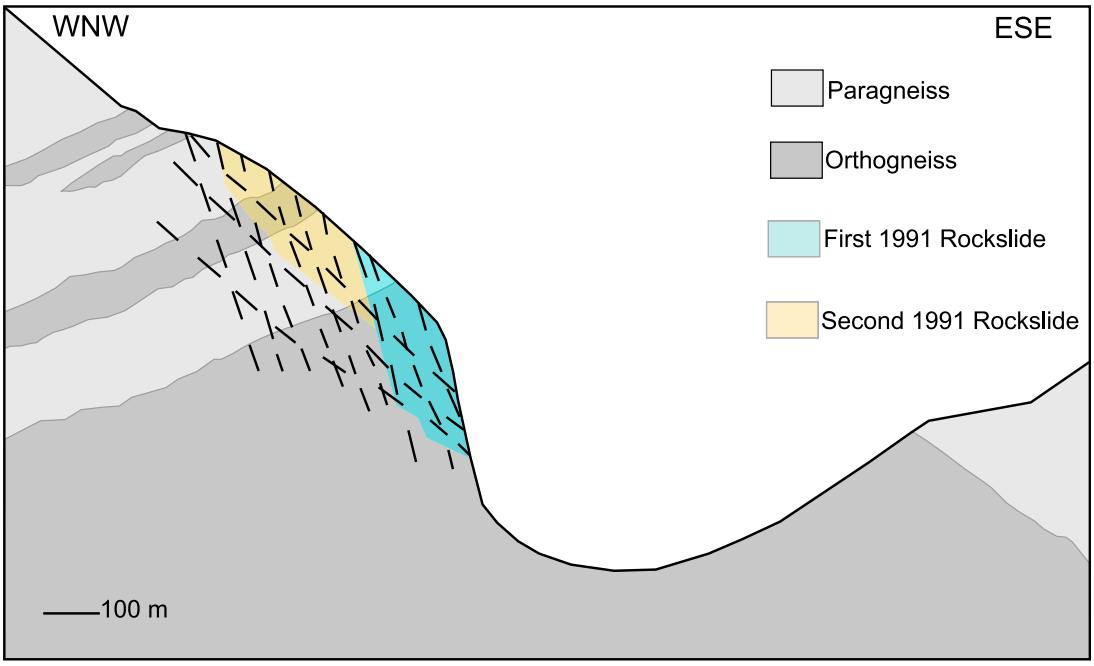

Figure 1. Synthetic cross section of the Grossgufer hillside before the two 1991 rockslides Modified from *Schindler et al.* [1993].

[*Agliardi et al.*, 2001]. The 1991 Randa failures occurred at the Grossgufer hillside, dominated by two gneiss formations (Figure 1). The Randa orthogneiss (locally called Randa augengneiss), located at the base of the hillside, is Permian porphyritic granite, affected by the alpine deformation. It is overlain by the Siviez Mischabel nappe paragneiss [*Bearth*, 1964; *Thélin*, 1987]. The Grossgufer cliff exhibits fracture zones formed during the late alpine orogeny. These fracture zones have been grouped into seven distinct sets [*Ischi et al.*, 1991; *Noverraz and Bonnard*, 1992; *Rouiller*, 1992; *Sartori et al.*, 2003]. Of these, two fracture zone sets can be observed along a WNW-ESE cross section [*Schindler et al.*, 1993]. With these two fracture sets, fracture is intense, but it remains challenging to get a full description of all fractures and their persistence [*Goodman and Shi*, 1985; *Wagner*, 1991; *Sartori et al.*, 2003; *Jaboyedoff et al.*, 2004; *Willenberg*, 2004; *Spillmann et al.*, 2007; *Willenberg et al.*, 2008]. In a simplified view of the hillside used for the physical modeling reported in this paper, the first set is represented as a series of nine subvertical fractures, and the second as three subhorizontal discontinuous fractures (Figure 1).

[4] In order to determine if this simplified representation of the fracture network reflects the real state of prefailure fracturing, we performed four groups of experiments. The topography was that of a west-east cross section of the Grossgufer hillside, derived from topographic maps. In a first set of experiments, we considered a homogeneous model which is assumed to be massive but homogeneously fractured, without any localized weak zones. In the second set, we imposed nine vertical and three horizontal preexisting fractures to represent two of the main fracture zones at Randa. All of these fractures were of equal length. In the third set of experiments, the length of fractures coinciding with the outline of the 1991 rockslide events was extended. This was done to test the role of fracture persistence within the slope. In the last set of experiments we removed fractures from the previous configuration that seemed from observation to play no role in the gravitational failure.

3. Experimental Setup and Procedure

[5] A complete description of the method used to create a model is given by *Bachmann et al.* [2004] and *Chemenda et al.* [2005]. A model is created by pouring a melt of the analog material slope 1 into a rigid box at a temperature of 50°C. Slope 1 is a low frictional elastobrittle plastic analog material with strain softening [*Chemenda et al.*, 2005]. This material represents a compositional system based on liquid and solid hydrocarbons. Slope 1 is custom-made and available from MIR International, Inc. (Newton, Massachusetts). In order to create the fractures a series of openings cut in the two opposite lateral sides of model box are used to position taut strings. After cooling to a temperature of 20°C, at which the crystallized material is strong enough to be easily handled without damage, strings are moved along the slots to cut the fractures, and then removed. The model surface is then planed to obtain the desired relief (Figure 2a). The sub vertical fractures have been numbered from V1 near the valley to V9 near to the summit. The subhorizontal fractures have been numbered from H1, for the shallowest, to H3 for the deepest (Figure 2b).

[6] Once the model is prepared it is loaded into a vertical accelerator table. The latter consists of a mobile platform that can be lifted up to 2 m and then released. During its free fall the model reaches a maximum velocity of 6 m s^{-1}. The platform is then rapidly but smoothly decelerated to zero velocity when it comes into contact with a progressive shock

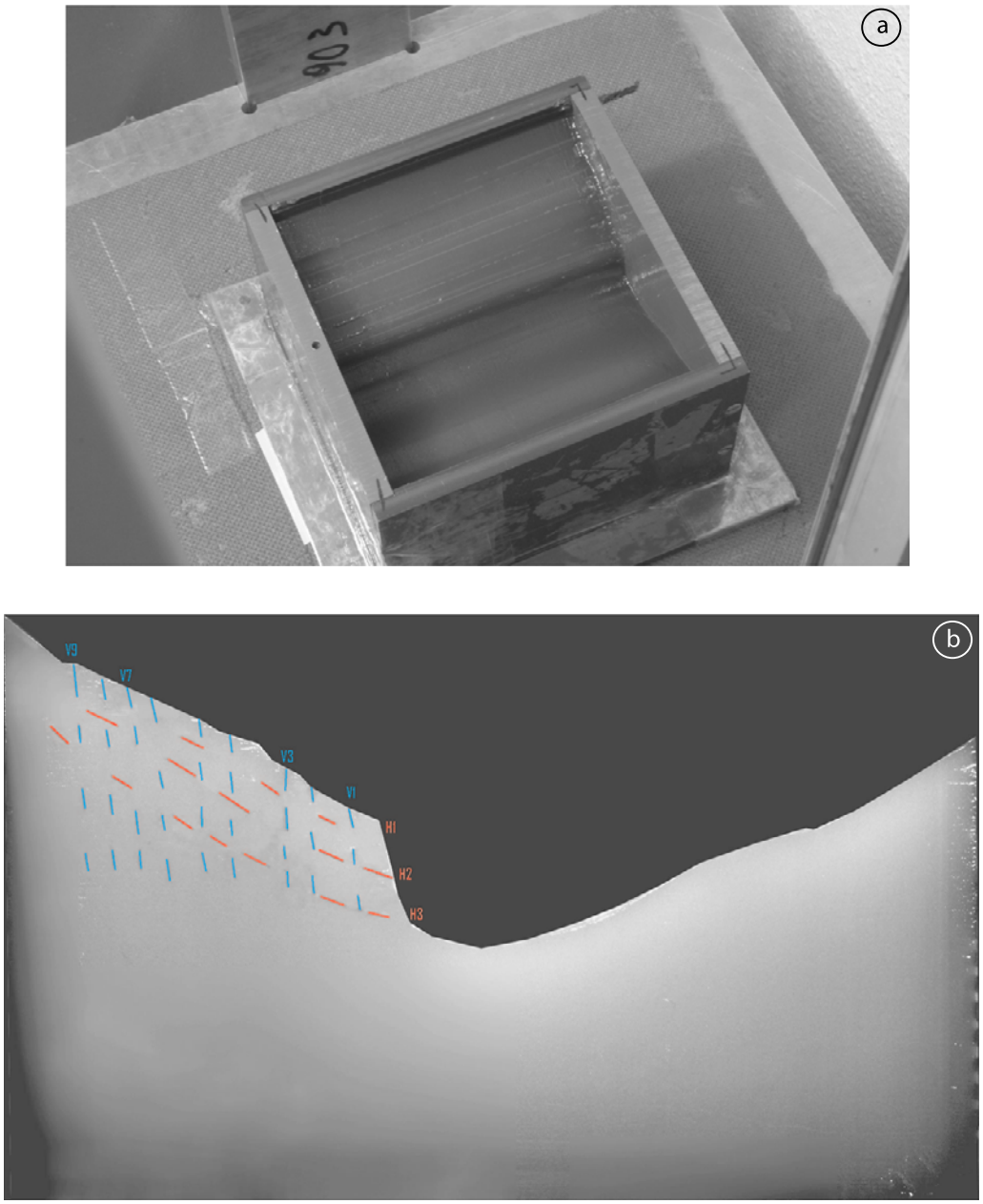

Figure 2. (a) View from above of the rigid box containing the model (0.14 × 0.14 m in section). This box is located on the mobile platform of the vertical accelerator, and (b) cross section of the model corresponding to the west-east cross section of the Grossgufer hillside. Vertical discontinuous fractures have been numbered from V1 near the valley to V9 near the summit and the subhorizontal fractures from H3 for the deeper to H1 for the shallower.

absorber of 5 cm stroke. During this phase the model undergoes a strong vertical deceleration (up to 500 m s^{-2}). This deceleration acting in the same direction as gravity is repeated until failure develops, usually ~100 cycles. Preliminary calibration tests are needed to determine which acceleration must be imposed to a model for a given configuration (geometry, prefracturing state…) in order to observe failure for a number of loading cycles ranging from 100 and 150. The main similarity criterion is

$$\frac{\sigma_c^o}{\rho^o g^o H^o} = \frac{\sigma_c^m}{\rho^m g^m H^m} \quad (1)$$

where $\rho\, g$ is the specific weight (ρ is density and g is gravity acceleration), σc is the strength under uniaxial compression, H is the spatial scale of the phenomenon (the mountain height H, for example) and superscripts "o" and "m" mean original and model, respectively. The scaling factor $\frac{H^o}{H^m}$ has been chosen to be 1/10,000, so that 1 cm in the model corresponds to 100 m in reality. Experiments were carried out at a fixed temperature of 20°C. In this condition slope 1 exhibits high softening with σ_c^m = 2500 Pa (Figure 3). This mechanical behavior is comparable to strength degradation behavior introduced in some numerical models [*Eberhardt et al.*, 2004; *Stead et al.*, 2006]. At this temperature the

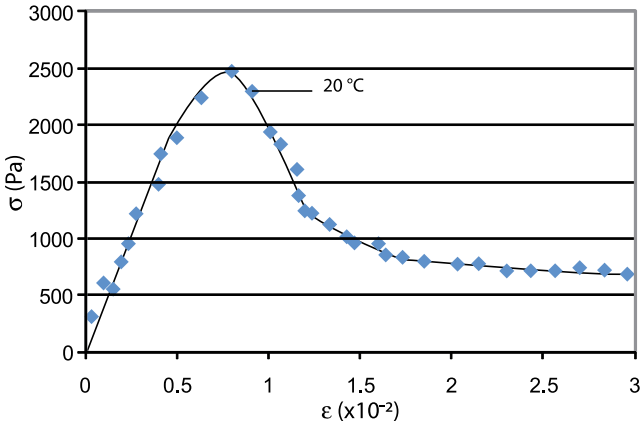

Figure 3. Uniaxial stress/strain diagram at temperature T = 20°C and $\dot{\varepsilon} = 10^{-2}s^{-1}$ showing the mechanical properties of the model material slope 1.

coefficient of friction measured on the preexisting fractures is $\mu = 0.2$.

[7] Using equation (1) for a given σ_c^m, the only free parameter that remains to satisfy the criteria is g^m, the acceleration experienced by the model. For a given model configuration the experiment was performed several times in order to determine an appropriate gm threshold, by increasing the acceleration, but altering the table drop height, between two experiments until unstable state was reached. The similarity criterion (1) was thus used to determine the effective compressive strength σ_c^o of the intact material at the mountain scale. Cross sections are made at the end of each experiment. The model is cooled to 5°C in order to increase its strengths and then cut in order to study the internal deformation. Some experiments were stopped in the early stages of model deformation to analyze the corresponding evolution of internal slope deformation.

4. Results

[8] A total of 50 experiments have been conducted under various conditions. We report here the results of the four most representative trials. Each of the experiments presented has been performed at least 5 times in order to ensure repeatability of the result. Mobilized volumes have been calculated in each case considering the mobilized surface (in m^2 given that 1 cm in the model corresponds to 100 m in nature/original) multiplied by 1 m width. Due to our 2-D modeling approach, those volumes are much smaller than those estimated from the 1991 Randa rockslide. Our purpose is thus only to compare the mobilized volume between experiments.

4.1. Experiment 1: Homogenous Model (Homogeneously Fractured at Scale)

[9] In this homogeneous configuration, rupture occurred at an acceleration of $g^m = 200$ m s^{-2}, imposed upon the model. Nonelastic deformation was first localized along two developing master faults that appear simultaneously and converge at the toe of the slope (Figure 4b). The thickness of the mobilized mass delimited by these faults is between 0.01 to 0.015m in the model, corresponding to 100 to 150 m in nature. No major fracturing is observed within the displaced sliding mass (Figure 4c). A single secondary fault then appears at the toe of the slope, and enables the volume to mobilize. In this homogeneous configuration the destabilization formed a deep seated landslide and not a retrogressing rockslide sequence. The total mobilized volume was 117,000 +/− 2,000 m^3.

4.2. Experiment 2: Highly Prefractured Model With Discontinuous Joints

[10] In this experiment we considered a model with nine discontinuous sub vertical fractures and three discontinuous sub horizontal fracture sets, dipping 30° east. All fractures (sub horizontal and subvertical) have a comparable initial

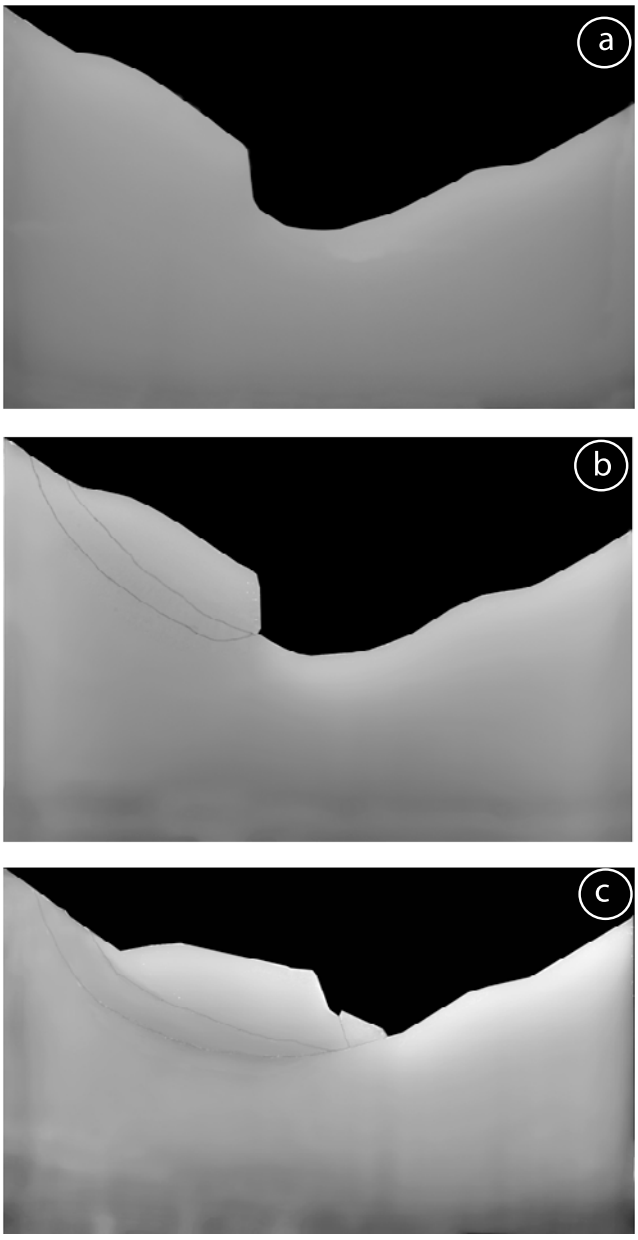

Figure 4. Experiment 1. (a) Initial homogeneous model, (b) cross section realized at an early stage of evolution (after 100 acceleration stages), and (c) cross section realized at an advanced stage of evolution (after 120 acceleration stages).

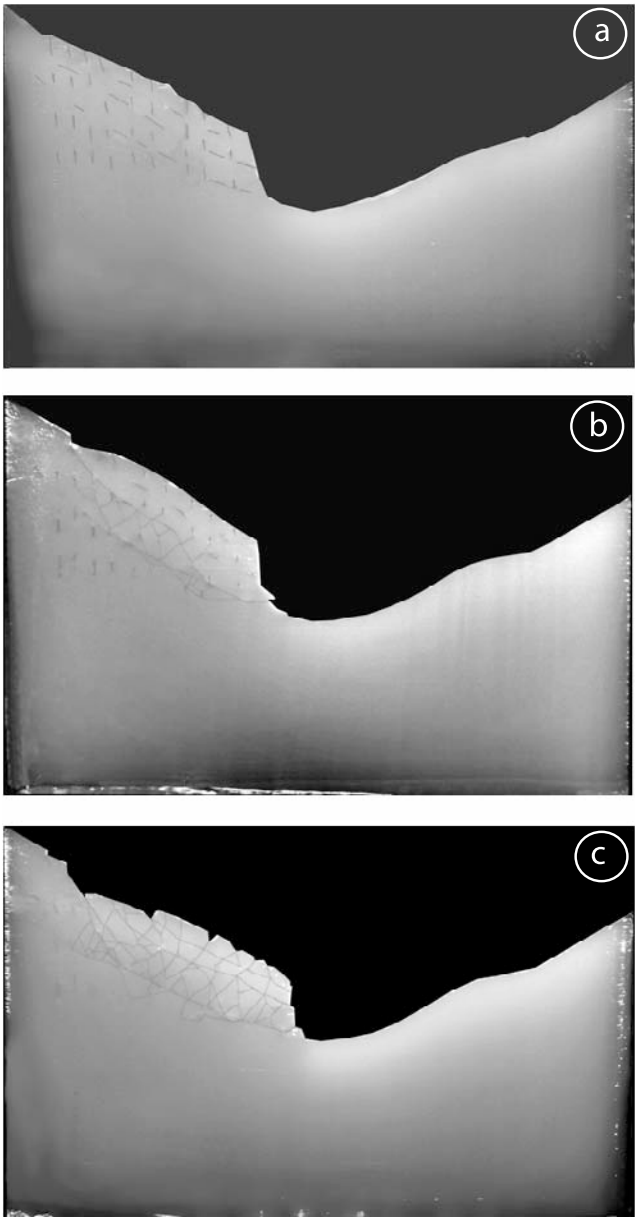

Figure 5. Experiment 2. (a) Initial highly prefractured model with discontinuous same length joints, (b) cross section realized at an early stage of evolution (after 100 acceleration stages), and (c) cross section realized at an advanced stage of evolution (after 120 acceleration stages).

size of about 0.005 m, representing discontinuities with persistence of approximately 50 m in nature (Figure 5a). The acceleration needed to destabilize the model was g^m = 180 m s^{-2}. In the early stage of failure the location of nonelastic deformation location lies close to that observed in experiment 1 (Figure 5b). We observed the formation of two master faults converging at the slope toe (compare Figures 4b and 5b). We can estimate the depth of the shallowest fault to be 100 m and 170 m for the deepest. The location and shape of the faults is controlled by the two deepest discontinuous horizontal fractures (H2 and H3). Furthermore, a large number of secondary fractures formed between the two master faults. We can observe that the deepest master fault became wider as shear displacement increased. At an advanced deformation stage (Figure 5c) all fractures propagated, defining small blocks sliding coherently in a deep seated landslide manner. The total mobilized volume was 71,000 +/− 2,000 m^3.

4.3. Experiment 3: Highly Prefractured Model With Some Continuous Joints

[11] In order to test the influence of fracture persistence on rockslide initiation, the length of some fractures was doubled (Figure 6a). We chose to increase the length of the fractures

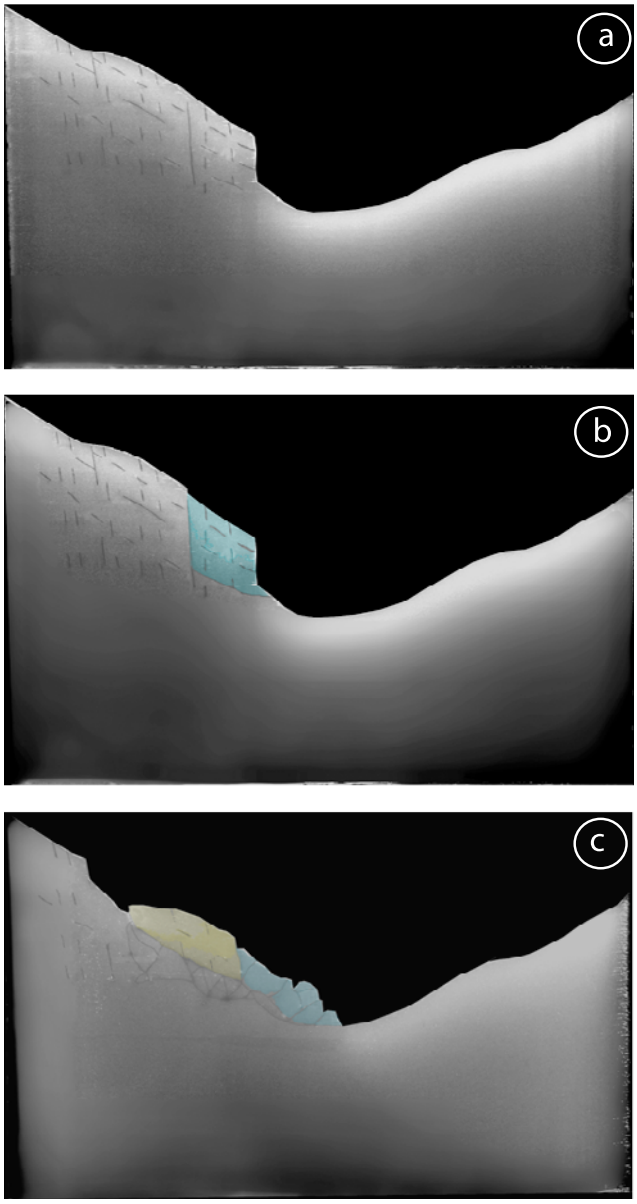

Figure 6. Experiment 3. (a) Initial highly prefractured model with some continuous joints. In this case the fractures assume to have initiated the two Randa rockslides are longer than any others. (b) Cross section realized at an early stage of evolution (after 100 acceleration stages). The first block is in blue and the second one in yellow. (c) Cross section realized at an advanced stage of evolution (after 120 acceleration stages).

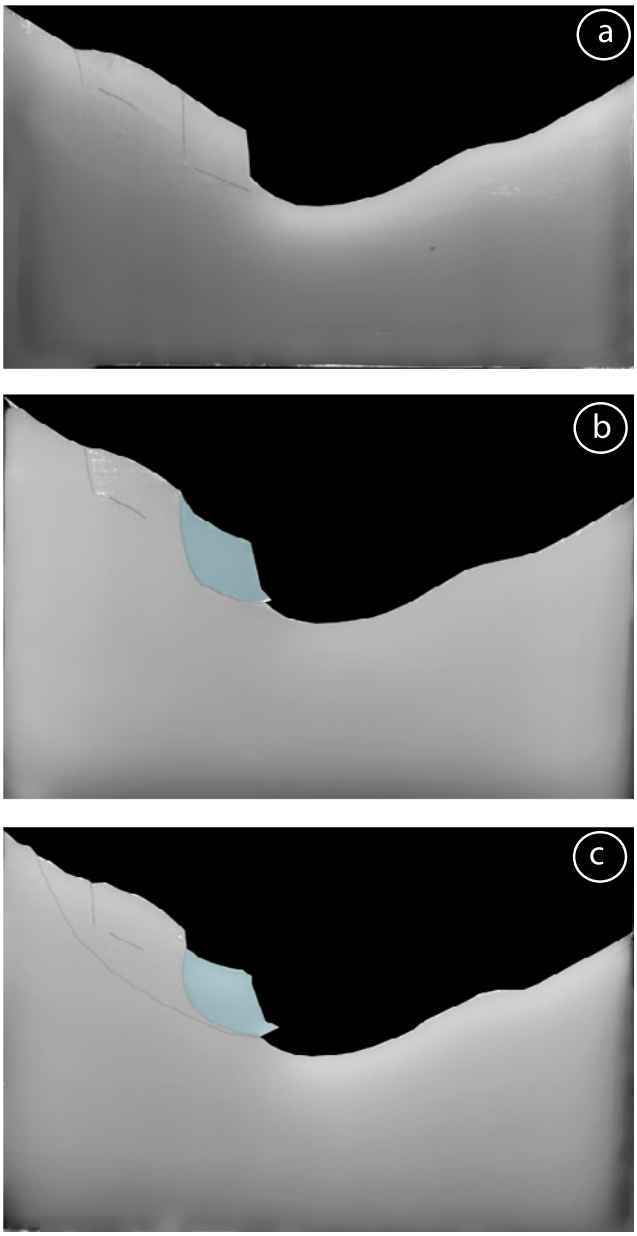

Figure 7. Experiment 4. (a) Initial slightly prefractured model, (b) cross section realized at an early stage of evolution (after 100 acceleration stages), and (c) cross section realized at an advanced stage of evolution (after 120 acceleration stages).

identified previously as those that delimit the two 1991 rockslides events at Randa. In this model the acceleration necessary to generate rupture was g^m = 150 m s^{-2}. During early deformation we observed (Figure 6b) that the two long fractures, V3 and H3 close to the slope toe, connect to release a single destabilized block, colored blue in Figure 6b). At this stage, the deformation is defined purely by these two fractures. The location and geometry of the resultant mobilized block corresponds well to the first 1991 Randa rockslide. During an advanced deformation stage (Figure 6c), the sliding surface of the first mobilized block propagates to the left side of the 215 model. A second block above the first then becomes unstable, labeled in yellow in Figure 6c. The location of the second mobilized block again corresponds well to the second failure in 1991 at Randa. Inside the first block, the preexistent fractures propagate and ultimately delimit some smaller blocks that fall to the valley as rockfalls. In this experiment we observed that only a few fractures were activated during the model destabilization. The total mobilized volume in this model was 68,000 +/− 2,000 m^3.

4.4. Experiment 4: Partially Prefractured Model With Continuous Joints

[12] Due to the previous model result, we consider the relative importance of fractures and hence which fractures control and define failure development. To approach this question we removed the inactive fractures from the previous model configuration (Figure 7a). In this test the model failed at acceleration of g^m = 190 m s^{-2}. In the early stage of deformation the two fractures V3 and H3 still propagated and delimit a block corresponding to the first 1991 Randa rockslide, labeled in blue in Figure 7b. When the loading was increased, nonelastic deformation localized along a master fault connecting the base of this block and the top surface of the model (Figure 7c). The two fractures V7 and H2 were not involved in the formation of the master fault, nor in the evolving model destabilization. The total mobilized volume in this test was 70,000 +/− 2,000 m^3.

5. Discussion

[13] Our modeling approach provides a technique to determine and constrain large-scale rock mass strength parameters [*Goodman*, 1980; *Brady and Brown*, 1985; *Hoek and Brown*, 1997]. This is undertaken by studying the deformation of a given model configuration subject to a progressively increased gravitational loading g^m. The effective compressive strength of the rock mass at the mountain scale, σ_c^o, is determined by the similarity criterion (equation (1)), considering a scaling factor The scaling factor $\frac{H^o}{H^m}$ = 1/10,000 and $\rho^m = 0.86 \times 10^3$ kg m^{-3} and assuming that ρ^o = 2500 kg m^{-3}. For a homogeneous model the effective compressive strength of the rock mass at the mountain scale was σ_c^o = 11 MPa. In the case of intensively prefractured model with discontinuous joints it was σ_c^o = 13 MPa, and σ_c^o = 14 MPa with limited continuous joints. The partially prefractured configuration with continuous joints derives an effective compressive strength of σ_c^o = 12 MPa. The results indicate that the introduction of fractures results in easier destabilization of the mountain, that is, sliding occurs at higher σ_c^o values and hence for a lower acceleration g^m. The difference between prefractured models and homogeneous one is however not drastic. Furthermore, the computed effective compressive strength values correspond well to those obtained from numerical models [*Eberhardt et al.*, 2004; *Stead et al.*, 2006]. Fractures and their persistence facilitate gravitational failure and have an influence on the final mobilized volume. There is a difference between the volume mobilized in the homogenous case (about 117,000 m^3) and the three prefractured cases, for, which the total mobilized volume ranged from 68,000 m^3 to 71,000 m^3. However, the persistence of fractures also had a significant influence on the dynamics of the movement (deep seated landslide versus retrogressive rockslide), yet

had no influence on the resulting mobilized volume. The mobilized volume is more closely dependant on the combined influence of topography and preexisting fractures, as proposed by *Jaboyedoff et al.* [2004], rather than on their persistence. Both physical and numerical models indicate that the mobilized volume is delimited by the localization of irreversible plastic deformation at depth. The latter corresponds to the location of the two master faults (Figure 2b), and to the zones of high shear stress intensity as shown in numerical models [*Eberhardt et al.*, 2004]. Regarding the mobilized volume, the discrepancy between the homogeneous and other prefractured cases could be explained as follows: the discontinuous fractures introduced in our models have been explicitly positioned at a depth, coinciding with the lower limit of the first 1991 rockslide. It is however plausible that fractures affect the massif more deeply. Introduction of such deep fractures in our models should result in an increasing depth of the main failure plane, and hence in increasing the mobilized volume until a threshold value defined here by the homogeneous case. In this last case we obtain a gravitational mobilized volume dissimilar to the 1991 event field observation. This suggests that at least one other mechanism not or only partially taken into account in these models could be involved in controlling gravitational slope failure, which could be the state of prefracturing. The main implication of this study is provided by the comparison of experiments 3 and 4. This clearly shows that fractures which seemed not have any role in the gravitational failure actually hold great influence on the kinematics of sliding. This indicates that an accurate knowledge of fracturing is necessary to understand deep seated gravitational slope failure mechanism. It remains difficult to identify any fracture and its persistence in the field, and even more so to introduce each fracture in a physical or numerical model. The prefracturing state of the slope is responsible for strength reduction of the superficial massif [*Chigira*, 2001; *Maréchal et al.*, 2003] due to fracturing itself, but also by weathering [*Girod*, 1999]. To confirm this, field observation on fracture density and rock strength characterization as a function of depth is needed. This rock strength variation should be then introduced into physical and numerical models, rather than any partial or explicit fracture set representation.

6. Conclusion

[14] This study focused on the influence of inherited structural heterogeneities (joints and fractures) on mountain slope destabilization. Our 2-D physical model experimental results identify some of the first-order parameters in controlling mountains destabilization and their relative influence. The first is the density of fractures; it has been demonstrated that an increase in the density of fractures facilitates gravitational failure and increases the resulting mobilized volume. The second one is fracture persistence; persistence of fractures had no influence on the volume of the mobilized mass, but holds a strong control over the kinematics of gravitational movements.

[15] Our results showed that the geometry of the fractures at depth have a great influence on the gravitational deformation of an actively failing hillside and on the resulting slope morphology. It is thus of first importance to determine not only the geometry of fracture networks affecting a mountain, but also their persistence at depth. It seems thus particularly important to determine if weathering and/or damage at shallow depth are needed to explain shallow rockslides widely observed in nature.

[16] **Acknowledgments.** Authors are really grateful to Nick Rosser for his help, useful suggestions, and corrections; to the reviewers for their constructive reviews that have led to a great improvement of the present article; and to Damien Bachmann for his suggestions and his help.

References

Agliardi, F., G. Crosta, and A. Zanchi (2001), Structural constraints on deep-seated slope deformation kinematics, *Eng. Geol. Amsterdam*, *59*, 83–102, doi:10.1016/S0013-7952(00)00066-1.

Bachmann, D., S. Bouissou, and A. Chemanda (2004), Influence of weathering and pre existing large scale fractures on gravitational slope failure: Insights from 3-D physical modelling, *Nat. Hazards Earth Syst. Sci.*, *4*, 711–717, doi:10.5194/nhess-4-711-2004.

Bachmann, D., S. Bouissou, and A. Chemenda (2006), Influence of large scale topography on gravitational rock mass movements: New insights from physical modeling, *Geophys. Res. Lett.*, *33*, L21406, doi:10.1029/2006GL028028.

Bachmann, D., S. Bouissou, and A. Chemenda (2009), Analysis of massif fracturing during deep seated gravitational slope deformation by physical and numerical modelling, *Geomorphology*, *103*, 130–135, doi:10.1016/j.geomorph.2007.09.018.

Bearth, P. (1964), Geologischer Atlas der Schweiz-Erläuterungen zum Blatt Randa, 1:250,000, Kümmerly Frey, Bern.

Bois, T., S. Bouissou, and Y. Guglielmi (2008), Influence of major inherited faults zones on gravitational slope deformation: a two-dimensional physical modelling of the La Clapière area (Southern French Alps), *Earth Planet. Sci. Lett.*, *272*, 709–719, doi:10.1016/j-epsl_2008.06.006.

Brady, B. H. G., and E. T. Brown (1985), *Rock Mechanics for Undergroung Mining*, Allen and Unwin, St. Leonards, N.S.W., Australia.

Chemenda, A., S. Bouissou, and D. Bachmann (2005), 3-D physical modeling of deep-seated landslides: New technique and first results, *J. Geophys. Res.*, *110*, F04004, doi:10.1029/2004JF000264.

Chigira, M. (1985), Mass rock creep of crystalline schist: Minor structures formed by mass rock creep, *J. Jpn. Soc. Eng. Geol.*, *26*, 25–79.

Chigira, M. (2001), Micro-sheeting of granite and its relationship with landsliding specially after the heavy rainstorm in June 1999, Hiroshima prefecture, Japan, *Eng. Geol. Amsterdam*, *59*, 219–231, doi:10.1016/S0013-7952(00)00075-2.

Eberhardt, E., D. Stead, and J. Coggan (2004), Numerical analysis of initiation and progressive failure in natural rock slopes: The 1991 Randa rockslides, *Int. J. Rock Mech. Min. Sci.*, *41*, 69–87, doi:10.1016/S1365-1609(03)00076-5.

Einstein, H. H., D. Veneziano, G. B. Beacher, and K. J. O'Reilly (1983), The effect of discontinuity persistence on rock slope stability, *Int. J. Rock Mech. Min. Sci.*, *20*, 227–236.

Girod, F. (1999), Altération météorique de roche granitique en milieu alpin: Le cas de l'orthogneiss associé à l'éboulement de Randa (Mattertal, Valais, Suisse), Ph.D. thesis, 207 pp., Univ. Lausanne, Lausanne, Switzerland.

Goodman, R. E. (1980), *Introduction to Rock Mechanics*, John Wiley, Hoboken, N. J.

Goodman, R. E., and G. H. Shi (1985), *Block Theory and Its Application in Rock Engineering*, 338 pp., Prentice-Hall, Englewood Cliffs, N. J.

Hoek, E., and E. T. Brown (1997), Practical estimates of rock mass strength, *Int. J. Rock Mech. Min. Sci.*, *8*, 1165–1186.

Ischi, H., H. R. Keusen, and E. Scheller (1991), Bergsruz Grossgufer vom April/Mai 1991, Zusammenfassender Berichte über die Aktivität der Geotest, *Rep. 91126*, Geotest, Martigny, Switzerland.

Jaboyedoff, M., F. Baillifard, R. Couture, J. Locat, and P. Locat (2004), New insight of geomorphology and landslide prone area detection using DEM, in *Landslides Evaluation and Stabilization*, edited by W. A. Lacerda et al., pp. 199–205, A. A. Balkema, Rotterdam, Netherlands.

Kaneko, K., K. J. Otani, Y. Noguchi, and N. Togashiki (1997), Rock fracture mechanics analysis of slope failure, in *Deformation and Progressive Failure in Geomechanics*, edited by A. Asaoka et al., pp. 671–676, Elsevier, New York.

Kato, J., and S. Hada (1980), Landslides of the Yoshino-Gawa water system and its geological aspects, *Res. Rep. Kochi Univ. Nat. Sci.*, *28*, 127–140.

Maréchal, J. C., R. Wyns, P. Lachassagne, K. Subrahmanyan, and F. Touchard (2003), Anisotropie verticale de la perméabilité de l'horizon fissuré des aquifères de socle: Concordance avec la structure géologique des profils d'altération, *C. R. Geosci.*, *335*, 451–460, doi:10.1016/S1631-0713(03)00082-8.

Noverraz, F., and C. Bonnard (1992), L'écroulement Rocheux de Randa, prés de Zermatt, in *Proceedings of the 6th International Symposium on Landslides*, edited by D. H. Bell, pp. 165–192, A. A. Balkema, Rotterdam, Netherlands.

Rouiller, J.-D. (1992), L'éboulement de Randa, *Route et Trafic*, *92*(3), 373–376.

Sartori, M., F. Baillifard, M. Jaboyedoff, and J.-D. Rouiller (2003), Kinematics of the 1991 Randa rockslides (Valais, Switzerland), *Nat. Hazards Earth Syst. Sci.*, *3*, 423–433, doi:10.5194/nhess-3-423-2003.

Scavia, C. (1995), A method for the study of crack propagation in rock structures, *Geothechnique*, *45*, 447–463, doi:10.1680/geot.1995.45.3.447.

Schindler, C., Y. Cuenod, T. Eisenlohr, and C. L. Joris (1993), Die Ereignisse vom 18 April und 9 Mai 1991 bei Randa (VS) – eint atypischer Bergstruz in Raten, *Eclogae Geol. Helv.*, *86*(3), 643–665.

Spillmann, T., H. Maurer, H. Willenberg, K. F. Evans, B. Heincken, and A. G. Green (2007), Characterization of an unstable rock mass based on borehole logs and diverse borehole radar data, *J. Appl. Geophys.*, *61*, 16–38, doi:10.1016/j.jappgeo.2006.04.006.

Stead, D., and E. Eberhardt (1997), Developments in the analysis of footwall slopes on surface coal mining, *Eng. Geol. Amsterdam*, *46*, 41–61, doi:10.1016/S0013-7952(96)00084-1.

Stead, D., E. Eberhardt, and J. Coggan (2006), Developments in the characterization of complex rock slope deformation and failure using numerical modelling techniques, *Eng. Geol. Amsterdam*, *83*, 217–235, doi:10.1016/j.enggeo.2005.06.033.

Terzaghi, K. (1962), Stability of steep slopes in hard unweathered rock, *Geotechnique*, *12*, 251–270, doi:10.1680/geot.1962.12.4.251.

Thélin, P. (1987), Nature Originelle des gneiss oeillés de Randa, *Bull. Lab. Géol. Mineral. Geophys. Mus. Geol. Univ. Lausanne*, *290*, Lausanne.

Wagner, A. (1991), Bergstruz Grossgufer Randa – Etude structurale et géomécanique, Cent. de Rech. Sci. Fondam. et Appl. de Sion, Sion, Switzerland.

Willenberg, H. (2004), Geologic and kinematic model of a complex landslide in crystalline rock (Randa, Switzerland), Ph.D. thesis, Swiss Fed. Inst. of Technol., Zurich.

Willenberg, H., S. Loew, E. Eberhardt, K. F. Evans, T. Spillmann, B. Heincke, H. Maurer, and A. G. Green (2008), Internal structure and deformation of an unstable crystalline rock mass above Randa (Switzerland): Part I — Internal structure from integrated geological and geophysical investigations, *Eng. Geol.*, *101*, 1–14.

T. Bois and S. Bouissou, Géosciences Azur, UMR 6526, Université de Nice Sophia-Antipolis, F-06560 Valbonne, France. (bois@geoazur.unice.fr)